Journal of Alloys and Compounds 553 (2013) 338–342

Contents lists available at SciVerse ScienceDirect

Journal of Alloys and Compounds

journal homepage: www.elsevier.com/locate/jalcom

Preparation and photoluminescence characteristics of $In(OH)_3$:xTb^{3+} obtained by Microwave-Assisted Hydrothermal method

F.V. Motta [a,*], A.P.A. Marques [b], M.S. Li [c], M.F.C. Abreu [d], C.A. Paskocimas [a], M.R.D. Bomio [a], R.P. Souza [e], J.A. Varela [f], E. Longo [d]

[a] DEMAT, CT, UFRN, Av. Sen. Salgado Filho 3000, CEP 59072-970 Natal, RN, Brazil
[b] UNIFESP, Rua Prof. Artur Riedel 275, CEP 09972-270 Diadema, SP, Brazil
[c] IFSC, USP, Av. Trabalhador São Carlense 400, CEP 13566-590 São Carlos, SP, Brazil
[d] LIEC, DQ, UFSCar, Via Washington Luiz, km 235, CEP 13565-905 São Carlos, SP, Brazil
[e] DEP, CT, UFRN, Av. Sen. Salgado Filho 3000, CEP 59072-970 Natal, RN, Brazil
[f] LIEC, IQ, UNESP, Rua Francisco Degni s/n, CEP 14801-907 Araraquara, SP, Brazil

ARTICLE INFO

Article history:
Received 22 May 2012
Received in revised form 2 November 2012
Accepted 10 November 2012
Available online 19 November 2012

Keywords:
Indium hydroxide
Terbium
Microwave-Assisted Hydrothermal

ABSTRACT

Crystalline terbium-doped indium hydroxide structures were prepared by a rapid and efficient Microwave-Assisted Hydrothermal (MAH) method. Nanostructures were obtained at a low temperature. FE-SEM images confirm that these samples are composed of 3D nanostructures. XRD, optical diffuse reflectance and photoluminescence (PL) measurements were used to characterize the products. Emission spectra of terbium-doped indium hydroxide ($In(OH)_3$:xTb^{3+}) samples under excitation (350.7 nm) presented broad band emission referent to the indium hydroxide matrix and $^5D_4 \rightarrow {}^7F_6$, $^5D_4 \rightarrow {}^7F_5$, $^5D_4 \rightarrow {}^7F_4$, and $^5D_4 \rightarrow {}^7F_3$ terbium transitions at 495, 550, 590 and 627 nm, respectively. Relative intensities of the Tb^{3+} emissions increased as the concentration of this ion increased from 0, 1, 2, 4 and 8 mol%, of Tb^{3+}, but the luminescence is drastically quenched for the $In(OH)_3$ matrix.

1. Introduction

Self-assembled micro-, meso- and nanostructures with specific morphologies, novel properties and great application potential in many fields are of great interest to chemists and material scientists because of their fundamental significance for addressing some basic issues of the quantum confinement effect and space-confined transport phenomena as well as their potential applications as advanced materials in functional nanodevices [1].

The indium hydroxide semiconductor with a wide band gap (E_g) estimated to be 5.15 eV is attractive due to its electronic and optical properties [2,3]. Recently, Shi et al. [4] reported a $In(OH)_3$ truncated polyhedral microcrystal formation via conventional hydrothermal treatment at 180 °C for 16 h and 18 h that showed PL spectrum with two emission peaks at 496.6 and 419.2 nm using an excitation wavelength (380 nm at room temperature). Yan et al. [3] showed a broad band PL blue–green emission peak of $In(OH)_3$ nanocubes centered at 480 nm.

Rare earth ions such as Tb^{3+} can be added in semiconductors to increase PL. Inorganic matrixes doped with Tb ions have been extensively studied due to optical properties of these ions; they could be extensively used as activators of the blue green emissions originate from the $^5D_3 \rightarrow {}^7F_j$ and $^5D_4 \rightarrow {}^7F_j$ transitions. A large number of blue and green phosphors composed of rare earths such silicates, aluminates and phosphates have been investigated [5–7].

Gaponenko et al. [8] showed Er^{3+} and Tb^{3+} doped In_2O_3 films fabricated on porous silicon synthesized by Sol–Gel. The compositions coating porous silicon are considered as promising host materials for erbium and terbium optical activation, allowing to detect both visible and infrared luminescence from samples annealed at low temperatures.

Indium hydroxides with different morphologies such as spheres [9], flowers [10], cubes [11–13], rods [14,15], etc., have been synthesized by several synthesis methods. The physical and chemical properties of these powders can be influenced by shape, size and size distribution of the particles which depend on the synthesis method. A conventional hydrothermal synthesis has been used to obtain structures of $In(OH)_3$ using a simple, practical and environmentally friendly method [3,9,16].

Komarneni et al. [17] introduced the use of microwave radiation in the hydrothermal system by promoting the development of a new technique offering reaction kinetic enhancement, formation of materials with different morphologies, low synthesis temperature and reduced processing times. Recently, the MAH method was successfully employed to obtain $In(OH)_3$ [13] and other oxides such as ZnO [18], $BaTiO_3$ [19], CuO [20], $BaMoO_4$ [21].

* Corresponding author. Tel.: +55 84 3342 2512; fax: +55 84 3342 2406.
E-mail address: fabiana@ct.ufrn.br (F.V. Motta).

0925-8388/$ - see front matter © 2012 Elsevier B.V. All rights reserved.
http://dx.doi.org/10.1016/j.jallcom.2012.11.063

In this paper, we report the synthesis of $In(OH)_3$:xTb^{3+} structures with concentrations of x = 0, 1, 2, 4 and 8 mol% of Tb^{3+} using the MAH method at a low temperature of 140 °C for 30 min. The architectures of $In(OH)_3$:xTb^{3+} as well as the morphology and PL properties of these samples were investigated.

2. Experimental

Using the MAH method, $In(OH)_3$ powders were obtained. For this synthesis, 3.6 Mmol of Indium (III) chloride (99% purity, Aldrich) and terbium nitrate were dissolved in 80 mL of deionized water under constant stirring. The ion Tb^{3+} was added in the following percentages: 0, 1, 2, 4 and 8 mol%. The pH of the solution was adjusted to 10 by adding NH_4OH. After stirring for 10 min, 1 mL of polyethyleneglycol PEG (Mw 600) was added to the solution, and the mixture was then transferred to a Teflon autoclave. The system was sealed and placed into a domestic microwave oven (2.45 GHz, maximum power of 800 W). The system consists of: (a) drilling of a 3 mm diameter opening in the upper part of the oven cavity for the passage of a thermocouple, (b) magnetron control by an external temperature controller, and, (c) addition of the microwave cell (apparatus developed for this purpose) within the cavity of the oven. The thermocouple is connected to an external controller, which receives the information of oven temperature from the thermocouple and controls the activity of the oven magnetron [22]. The reaction system was heat treated at 140 °C for 30 min (heating rate fixed at 25 °C/min) to all percentages added of terbium of the $In(OH)_3$.

The autoclave was cooled to room temperature naturally. A white product was separated by centrifugation, washed with deionized water and ethanol and dried at 60 °C in air. The powders were characterized by X-ray diffraction (XRD) using a Rigaku diffractometer (Model D/max-2500/PC) with Cu Kα radiation. The $In(OH)_3$ morphology and size were observed by field emission scanning electron microscopy (FE-SEM; Jeol JSM 6330F) images. UV–Vis reflectance spectra of $In(OH)_3$ powders were taken using Cary 5G equipment. PL spectra were measured using a Thermal Jarrel-Ash Monospec 27 monochromator and a Hamamatsu R446 photomultiplier. The 350.7 nm line of a krypton ion laser (Coherent Innova 90 K) was used as the excitation source with the output power of the lasers kept at 200 mW. All measurements were taken at room temperature.

3. Results and discussion

$In(OH)_3$ powders were synthesized with different percentages of Tb^{3+} at 140 °C for 30 min. X-ray diffraction was used to verify the crystal structures and purity of the samples. Fig. 1(a–e) shows XRD patterns of $In(OH)_3$:xTb^{3+} powders. All diffraction peaks present in XRD patterns could be indexed to the cubic lattice related to the $In(OH)_3$ phase (JCPDS card No. 16-0161). With terbium percentage increments (Fig. 1b–e), the phases obtained by MAH treatment remained $In(OH)_3$ with a cubic structure, which indicates the substitution of Tb^{3+} in the In^{3+} sites. No other phases, such as InOOH or In_2O_3, were verified. The absence of deleterious phases indicates the purity of the samples.

Table 1 presents the lattice constants, the volume cell and the average crystallite size (D_{crys}) of $In(OH)_3$:xTb^{3+} powders. The lattice parameters a were calculated using the least-square refinement

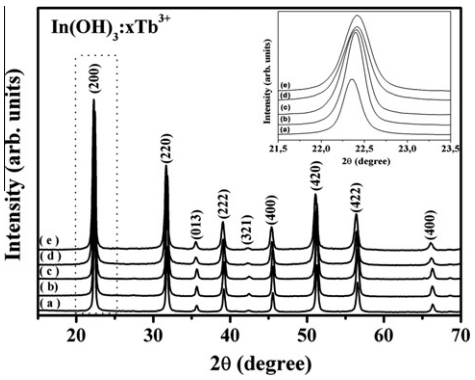

Fig. 1. XRD patterns of $In(OH)_3$:xTb powders obtained by the MAH method at 140 °C for 30 min: (a) x = 0, (b) x = 1, (c) x = 2, (d) x = 4 and (e) x = 8 mol%. The peaks (220) are shown in inset.

Table 1
Lattice constants (a, Å), cell volumes (V, Å^3) and the average crystallite size (D_{crys}, Å) of the cubic structure of $In(OH)_3$:xTb powders prepared by the MAH method.

$In(OH)_3$:xTb (mol%)	a (Å)[a]	V (Å^3)[a]	D_{crys} (Å)[a]
x = 0	7.9589(4)	504.15(7)	37
x = 1	7.9591(4)	504.19(7)	34
x = 2	7.9674(4)	505.78(7)	30
x = 4	7.9799(4)	508.15(7)	24
x = 8	7.9859(4)	509.29(7)	24

[a] Calculated using the (200) 100% diffraction peak.

from the UnitCell-97 program [23] as obtained from peak positions displayed in Fig. 1. The pure $In(OH)_3$ matrix contained lattice parameter a = 7.9589(4) Å which was visible as an increase in these values with an increase in the percentage of ion Tb^{3+}, especially for the 8 mol% Tb^{3+} sample where 7.9859(4). These observations are agreement with the investigation realized by Aliabad et al. using density functional theory (DFT) [24]. Aliabad et al. showed in their work that the lattice parameters in In_2O_3 matrix expand as a function of expansion of dopant ionic radii. In this work, both In^{3+} and Tb^{3+} ions have coordination number 8, and effective ionic radii expansion occurs in the following order: In^{3+} (106 pm) < Tb^{3+}(118 - pm) [25]. Therefore, is expected that the lattice parameters increase with an increase of Tb^{3+} ion contained in the $In(OH)_3$ matrix.

On the other side, the crystallite size decreased with Tb doping level, from 37 nm for pure $In(OH)_3$ to 24 nm for 8 mol% Tb^{3+}. Such behavior can be explained by the fact that the increase of Tb doping level was accompanied with the increase in number of lattice defects in hydroxide (Tb^{3+} cations and interstitial O^{2-} anions, respectively), which increased the lattice strain and disturbed the crystallites to grow. Such behavior is reminiscent of Vegard's law for two-component metal solid solutions, which predicts that the cell dimensions of the solid solution vary linearly with the concentration of the solute component [26]. Expansion in lattice parameters have been observed with decreasing crystallite sizes in many nanocrystalline oxides such as CeO_2, Fe_2O_3, MgO, TiO_2 (rutile),and ZrO_2 [27–32].

To our knowledge, the optical properties of $In(OH)_3$:xTb^{3+} have rarely been studied. Figs. 2 and 3 show absorbance and PL spectra of $In(OH)_3$:xTb^{3+} structures at room temperature. Efficient green emission can be observed when the $In(OH)_3$ matrix is doped with Tb^{3+}, showing a potential application for the nanoarchitectures to serve as efficient green phosphor in luminescent nanodevices. Much interest has been dedicated to the study of PL in nanostructural materials since the first visible PL at room temperature was observed in porous silicon for the first time [33]. Rare ions are used to dope oxides not only as a probe to investigate local centers and energy [34–36], but also to provoke changes in the optical behavior.

Optical diffuse reflectance measurements have been carried out on $In(OH)_3$:xTb^{3+} particles obtained under MAH conditions. An estimation of the optical band gap "E_{gap}" was obtained using the Wood & Tauc method [37]. The calculated values of E_{gap} were 5.12, 5.06, 5.12, 4.77 and 4.90 eV for the samples treated at 140 °C for 30 min, pure and with 1, 2, 4 and 8 mol% Tb^{3+}, respectively. Fig. 2 shows that the increase of the percentage of ion Tb^{3+} leads to a reduction in the E_{gap}. The E_{gap} of the pure indium hydroxide cube-like (E_{gap} = 5.12 eV) is like the $In(OH)_3$:xTb (E_{gap} = 4.90 eV − 8%Tb). Pure $In(OH)_3$ or $In(OH)_3$:xTb belongs to n-type semi-conductors where oxygen vacancies can induce the formation of new energy levels in the band gap. Thus, during the MAH process, the displacement of oxygen related to the In or Tb modulates different species of trapped holes ($V_O^{\bullet}$, V_O^{x} and $V_O^{\bullet\bullet}$ species) around $[InO_5 \cdot V_O^{x}]$ clusters and gives rise to complex cluster vacancies [18]. Before donor excitation, a hole in the acceptor and an

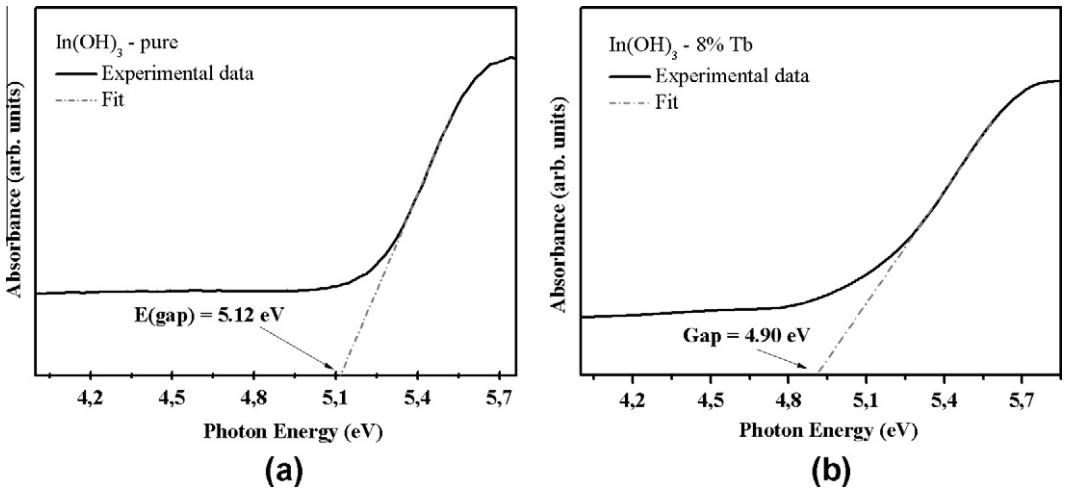

Fig. 2. UV–Vis absorbance spectra for the $In(OH)_3$:*x*Tb powders processed by the MAH method at 140 °C for 30 min: (a) *x* = 0 and (b) *x* = 8 mol%.

electron in a donor are created according to the following equations, where a Kröger–Vink notation is used for complex clusters [38]:

$$[InO_6]^x + \left[InO_5 \cdot V_o^x\right] \rightarrow [InO_6]' + \left[InO_5 \cdot V_o^{\bullet}\right], \quad (1)$$

$$[InO_6]^x + \left[InO_5 \cdot V_o^{\bullet}\right] \rightarrow [InO_6]' + \left[InO_5 \cdot V_o^{\bullet\bullet}\right], \quad (2)$$

$$[InO_6]' + [TbO_8]^{\bullet} \rightarrow [InO_6]^x + [TbO_8]^x, \quad (3)$$

$$\left[InO_5 \cdot V_o^{\bullet\bullet}\right]' + [TbO_8]^x \rightarrow \left[InO_5 \cdot V_o^{\bullet}\right]^x + [TbO_8]^{\bullet}|. \quad (4)$$

where $[InO_6]'$ and $[TbO_8]^x$ are donors; $\left[InO_5 \cdot V_o^{\bullet}\right]$ are donors/acceptors and $\left[InO_5 \cdot V_o^{\bullet\bullet}\right]$ and $[TbO_8]^{\bullet}$ are acceptors.

Fig. 3 depicts room temperature emission spectra of $In(OH)_3$:*x*Tb^{3+} powders prepared by the MAH method, heat-treated at 140 °C for 30 min, λEX 350.7 nm. Assuming the PL emission peaks can be described with a Gaussian function, the emission envelope in Fig. 3(i) can be fitted to multiple peaks. In the emission envelope from pure $In(OH)_3$, each color represents a different type of electronic transition and can be linked to a specific structural arrangement [39]. The pure $In(OH)_3$ matrix PL curves for all samples are composed of four PL components with the following nm maxima: blue = 450 nm, green = 512 nm, yellow = 570 nm and orange = 623 nm. Green maximum percentage area was observed for the pure $In(OH)_3$. This study of $In(OH)_3$:*x*Tb^{3+} powder emission shows that increases in terbium concentration promote changes in the $In(OH)_3$:*x*Tb^{3+} emission properties related to $[TbO_8]^{\bullet}$ clusters (Fig 3ii). These materials produced the predominant band at around 550 nm (the $^5D_4 \rightarrow {}^7F_5$ transition of Tb^{3+}) which is responsible for its green emission. In the emission spectra of samples, another weaker emission at around 495 nm were assigned to the $^5D_4 \rightarrow {}^7F_6$ transition; the emission at around 590 nm was attributed to the $^5D_4 \rightarrow {}^7F_4$ transition, and the group emission at around 627 nm were assigned to the $^5D_4 \rightarrow {}^7F_3$ transition of the Tb^{3+} ions [40].

The emission spectrum are dominated by the peak at around 550 nm ascribed to the Tb^{3+} $^5D_4 \rightarrow {}^7F_5$ transition. This electric-dipole allowed transition is usually called as hypersensitive, so its intensity is strongly dependent on the Tb^{3+} surrounding, and it always will be dominant when Tb^{3+} is in the lattice site of noncentrosymmetric environment in the cube-like phases [5,41,42]. The $^5D_4 \rightarrow {}^7F_6$ transition however has a magnetic dipole character and its intensity is almost independent of the environment. In this way, the ratio of the $(^5D_4 \rightarrow {}^7F_5)/(^5D_4 \rightarrow {}^7F_6)$ emission intensity, gave us valuable information about the symmetry of the site in which Tb^{3+} ions are situated [42]. It was not observed significant changes in the ratio of the $(^5D_4 \rightarrow {}^7F_5)/(^5D_4 \rightarrow {}^7F_6)$, which were of around 0.007 for the samples having Tb^{3+} concentrations from 2 to 8 mol% Tb^{3+}, indicating that the Tb^{3+} surrounding in these samples is almost the same. The sample with 1 mol% of Tb^{3+}, however, presents the $(^5D_4 \rightarrow {}^7F_5)/(^5D_4 \rightarrow {}^7F_6)$ ratio of 0.03, accusing an increase in the symmetry of the Tb^{3+} site.

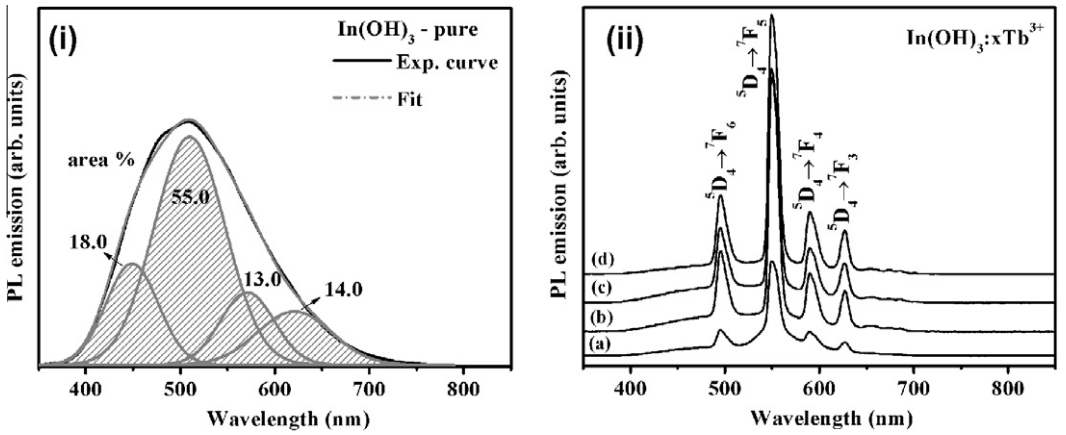

Fig. 3. PL spectra of $In(OH)_3$:*x*Tb structures obtained by the MAH method at 140 °C for 30 min: (i) *x* = 0 (deconvolution of a PL curve fitted) and (ii) (a) *x* = 1; (b) *x* = 2; (c) *x* = 4; (d) *x* = 8 mol%.

The relative intensities of the Tb^{3+} emissions increase as the concentration of this ion increases from 1 to 8 mol%; however the broad emission band of the $In(OH)_3$ cube-like clusters was not observed in $In(OH)_3$:xTb^{3+} powders. When the Tb^{3+} concentration is higher, the mechanism which prevails is the efficient energy transfer from the $In(OH)_3$ cube-like clusters to $[TbO_8]^{\bullet}$ clusters in these materials. This energy migration process is responsible for the increase in Tb^{3+} luminescence [42].

Fig. 4a–e depicts FE-SEM images of the $In(OH)_3$:xTb^{3+} nanostructures obtained at 140 °C for 30 min. Fig. 4a shows cubic and irregularly-shaped structures of pure $In(OH)_3$ with a smooth and uniform surface where the angle between the adjacent edges is relatively close to 90°; however, a difference in the morphology of the In(OH) which Tb^{3+} ion was apparent. It is seen clearly that the In(OH):xTb^{3+} (Fig. 4b–e) samples are composed of aggregated particles with medium-sized decrease and irregular morphology.

The experimental procedure used in the synthesis of $In(OH)_3$:xTb^{3+} in this work resulted in changes in the formation and morphology of the materials due to an intense and continuous nucleation–dissolution–recrystallization mechanism promoted by microwave hydrothermal processing [43,44], with transition from cubic shapes for random morphologies as can be seen in a schematic representation in Fig. 5.

Based on the FE-SEM micrograph, the material synthesized without the presence of Tb^{3+} ions, shows a cubic morphology well established and homogeneous, as shown in Fig. 5a. We believe that in this condition with only the presence of In^{3+} ions, the nucleation–dissolution–recrystallization mechanism does not occur in this syntheses due to the only changes of In^{3+} ions in the structure. However, when it is added 1% of Tb (Fig. 5b), can be seen the principle the nucleation–dissolution–recrystallization mechanism, where cubic structures of $In(OH)_3$ are dissolved and recrystallized in a different morphology due to presence of Tb^{3+} inside of the structure. As the concentration of Tb^{3+} is increases (Fig. 5b and c), notes that the cubic morphology of the $In(OH)_3$ starts to disappear and result in anisotropic growth and the formation of irregular morphology when the quantities of Tb^{3+} achieves 8%, as can be seen in Fig. 5e. At this point, the high concentration of Tb^{+3}, the lattice parameters in $In(OH)_3$ matrix expand as a function of expansion of dopant ionic radii Tb; therefore an increase of percentage

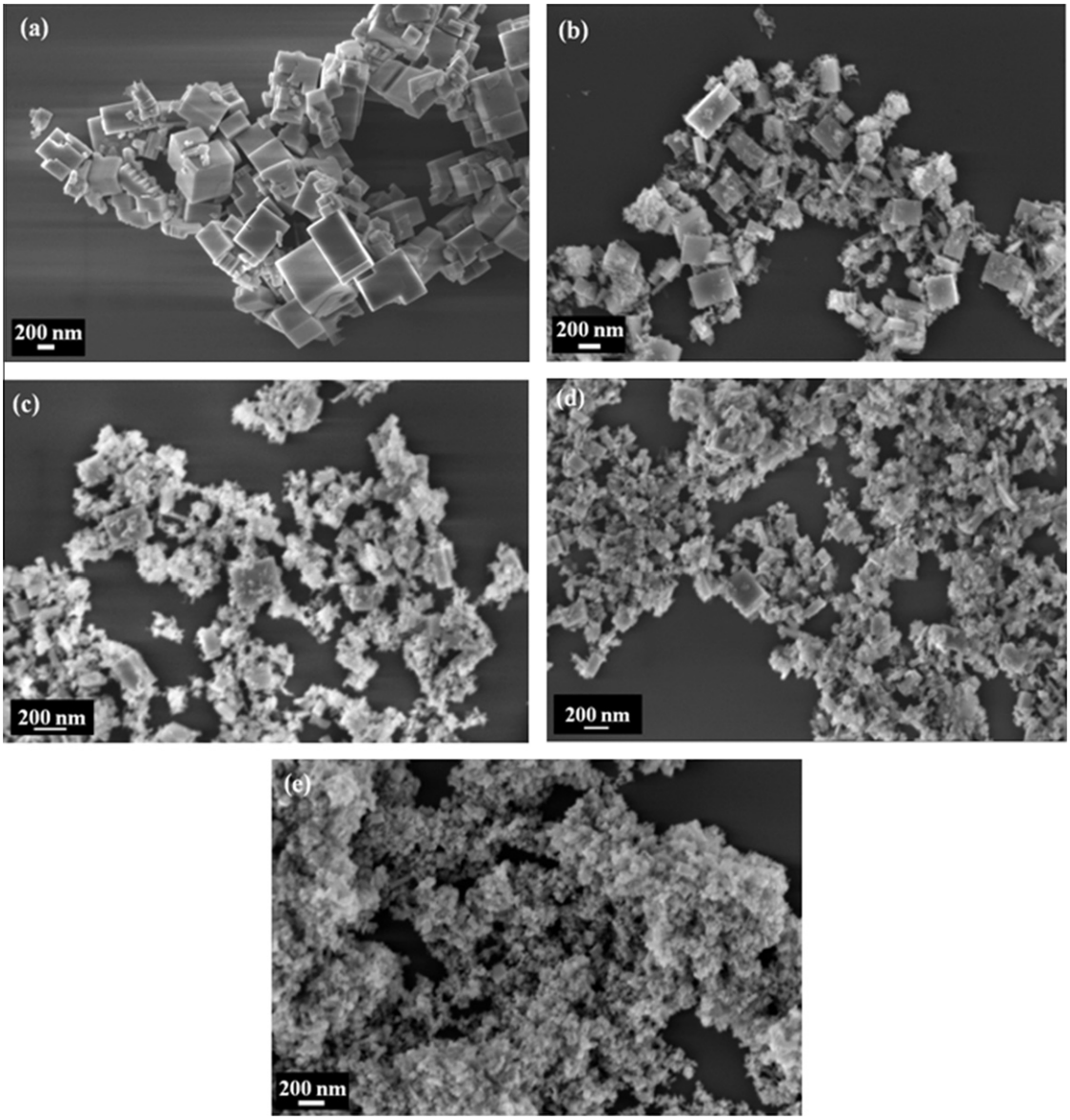

Fig. 4. FE-SEM images of the $In(OH)_3$:xTb powders: (a) $x = 0$, (b) $x = 1$, (c) $x = 2$, (d) $x = 4$ and (d) $x = 8$ mol%.

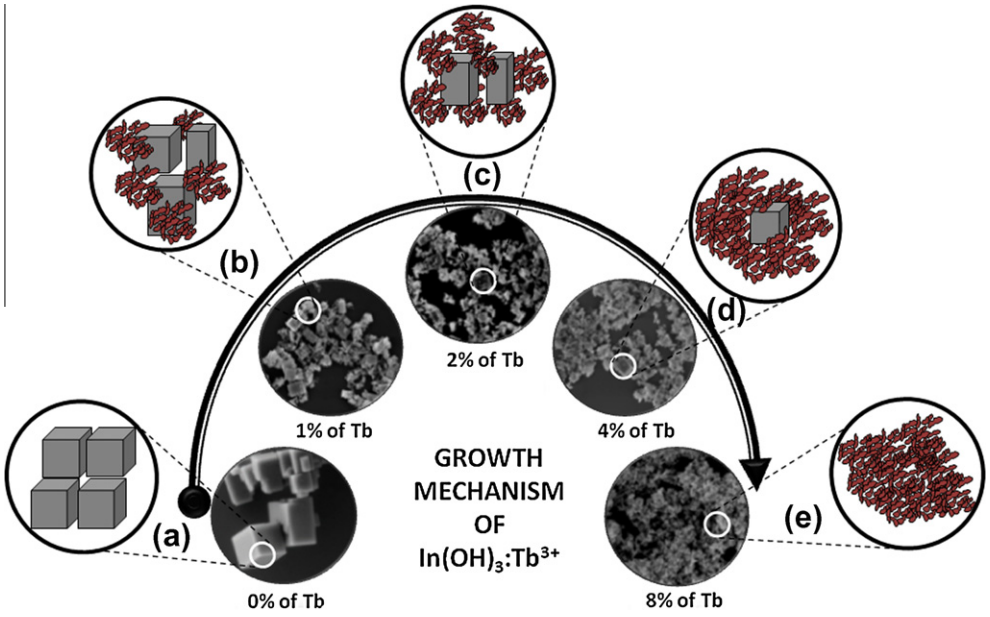

Fig. 5. Schematic representation of the change of morphologies of $In(OH)_3$:*x*Tb powders in function of Tb^{3+} concentrations: (a) $x = 0$, (b) $x = 1$, (c) $x = 2$, (d) $x = 4$ and (e) $x = 8$ mol%.

molar of Tb^{3+} ion contained in the arrangement can cause one more distortion of cubic lattice and consequently provoke one variation in morphology observed.

4. Conclusion

In(OH):*x*Tb^{3+} powders (where $x = 0$, 1, 2, 4 and 8 mol%) were efficiently obtained in their crystalline phase using the MAH method at 140 °C for 30 min. As shown in the FE-SEM images, increasing the percentage of terbium in the structure of $In(OH)_3$ influence the crystal size and morphology. The relative intensities of the Tb^{3+} ion emissions increase as the concentration of this ion increases from 1 to 8 mol% while in the $In(OH)_3$ matrix sample the luminescence intensity was drastically quenched. The mechanism which prevails in this case is the energy transfer from the $In(OH)_3$ matrix to one Tb^{3+}. These optical properties exhibited by In(OH):*x*Tb^{3+} suggest that this material is a highly promising candidate for photoluminescent applications.

Acknowledgements

The authors thank the financial support of the Brazilian research financing institutions: RECAM (*Rede de Catalisadores Ambientais*), CNPq and FAPESP-CEPID 98/14324-8.

References

[1] A.M. Cao, J.S. Hu, H.P. Liang, L.J. Wan, Angew. Chem. Int. Ed. 44 (2005) 4391.
[2] S. Avivi, Y. Mastai, A. Gedanken, Chem. Mater. 12 (2000) 1229.
[3] T.J. Yan, X.X. Wang, J.L. Long, P. Liu, X.L. Fu, G.Y. Zhang, X.Z. Fu, J. Colloid Int. Sci. 325 (2008) 425.
[4] Z. Shi, W. Wang, Z.K. Zhang, Mater. Lett. 62 (2008) 4293.
[5] Y. Liu, Z. Yang, Mater. Lett. 65 (2011) 1853.
[6] W. Zhi-Jun, L. Pan-Lai, Y. Zhi-Ping, G. Qing-Lin, J. Inorg. Mater. 26 (2011) 503.
[7] J.K. Han, G.A. Hirata, J.B. Talbot, J. McKittrick, Mater. Sci. Eng.: B 176 (2011) 436.
[8] N.V. Gaponenko, A.V. Mudryi, O.V. Sergeev, V.E. Borisenko, J.C. Pivin, A.S. Baran, E.A. Stepanova, A.I. Ratko, J.F. McGilp, Phys. Status Solidi A 165 (1998) 131.
[9] B.X. Li, Y. Xie, M. Jing, G.X. Rong, Y.C. Tang, G.Z. Zhang, Langmuir 22 (2006) 9380.
[10] H. Zhu, X.L. Wang, Z.J. Wang, C. Yang, F. Yang, X.R. Yang, J. Phys. Chem. C 112 (2008) 15285.
[11] F.V. Motta, R.C. Lima, A.P.A. Marques, E.R. Leite, J.A. Varela, E. Longo, Mater. Res. Bull. 45 (2010) 1703.
[12] F.V. Motta, R.C. Lima, A.P.A. Marques, M.S. Li, E.R. Leite, J.A. Varela, E. Longo, J. Alloys Comp. 497 (2010) L25.
[13] N. Koga, T. Kimizu, J. Am. Ceram. Soc. 91 (2008) 4052.
[14] L.A. Perez-Maqueda, L.F. Wang, E. Matijevic, Langmuir 14 (1998) 4397.
[15] L. Wang, L.A. Pérez-Maqueda, E. Matijevic, Colloid Polym. Sci. 276 (1998) 847.
[16] H.L. Zhu, N.Y. Wang, L. Wang, K.H. Yao, X.F. Shen, Inorg. Mater. 41 (2005) 609.
[17] S. Komarneni, R. Roy, Q.H. Li, Mater. Res. Bull. 27 (1992) 1393.
[18] R.C. Lima, L.R. Macario, J.W.M. Espinosa, V.M. Longo, R. Erlo, N.L. Marana, J.R. Sambrano, M.L.d. Santos, A.P. Moura, P.S. Pizani, J. Andrés, E. Longo, J.A. Varela, J. Phys. Chem. A 112 (2008) 8970.
[19] M.L. Moreira, G.P. Mambrini, D.P. Volanti, E.R. Leite, M.O. Orlandi, P.S. Pizani, V.R. Mastelaro, C.O. Paiva-Santos, E. Longo, J.A. Varela, Chem. Mater. 20 (2008) 5381.
[20] D.P. Volanti, D. Keyson, L.S. Cavalcante, A.Z. Simoes, M.R. Joya, E. Longo, J.A. Varela, P.S. Pizani, A.G. Souza, J. Alloys Comp. 459 (2008) 537.
[21] J.C. Sczancoski, L.S. Cavalcante, N.L. Marana, R.O. da Silva, R.L. Tranquilin, M.R. Joya, P.S. Pizani, J.A. Varela, J.R. Sambrano, M. Siu Li, E. Longo, J. Andrés, Curr. Appl. Phys. 10 (2010) 614.
[22] D. Keyson, D.P. Volanti, L.S. Cavalcante, A.Z. Simões, I.A. Souza, J.S. Vasconcelos, J.A. Varela, E. Longo, J. Mater. Process Technol. 189 (2007) 319.
[23] T.J.B. Holland, S.A.T. Redfem, Mineral. Mag. 61 (1997) 65.
[24] H.A.R. Aliabadi, H. Arabshahi, A.H. Aliabadi, Int. J. Phys. Sci. 7 (2012) 696.
[25] J.E. Huheey, E.A. Keiter, R.L. Keiter, Inorganic Chemistry: Principles of Structure and Reactivity, Prentice Hall, New York, 1997, p. 115.
[26] M.J. McKelvy, R. Sharma, A.V.G. Chizmeshya, R.W. Carpenter, K. Streib, Chem. Mater. 13 (2001) 921.
[27] M.I. Ahmad, S.S. Bhattacharya, Appl. Phys. Lett. 95 (2009) 191906.
[28] S. Tsunekawa, K. Ishikawa, Z.Q. Li, Y. Kawazoe, A. Kasuya, Phys. Rev. Lett. 85 (2000) 3440.
[29] P. Ayyub, V.R. Palkar, S. Chattopadhyay, M. Multani, Phys. Rev. B 51 (1995) 6135.
[30] A. Cimino, P. Porta, M. Valigi, J. Am. Ceram. Soc. 49 (1966) 152.
[31] G. Li, J. Boerio-Goates, B.F. Woodfield, L. Li, Appl. Phys. Lett. 85 (2004) 2059.
[32] H.K. Schmid, J. Am. Ceram. Soc. 70 (1987) 367.
[33] L.T. Canham, Appl. Phys. Lett. 57 (1990) 1046.
[34] H.M. Xiong, D.P. Liu, Y.Y. Xia, J.S. Chen, Chem. Mater. 17 (2005) 3062.
[35] S. Fujihara, Y. Ogawa, A. Kasai, Chem. Mater. 16 (2004) 2965.
[36] E.W. Draeger, J.C. Grossman, A.J. Williamson, G. Galli, J. Chem. Phys. 120 (2004) 10807.
[37] D.L. Wood, J.S. Tauc, Phys. Rev. B 5 (1972) 3144.
[38] F.A. Kröger, H.J. Vink, I.F. Seitz, D. Turnbull, Solid State Physics, Academic Press, New York, 1956.
[39] I.L.V. Rosa, A.P.A. Marques, M.T.S. Tanaka, F.V. Motta, J.A. Varela, E.R. Leite, E. Longo, J. Fluoresc. 19 (2009) 495.
[40] F. Shi, J. Meng, Y. Ren, Q. Su, J. Phys. Chem. Sol. 59 (1998) 105.
[41] A.P.A. Marques, F.V. Motta, M.A. Cruz, J.A. Varela, E. Longo, I.L.V. Rosa, Solid State Ion. 202 (2011) 54.
[42] Z. Li, J. Zeng, C. Chen, Y. Li, J. Cryst. Growth 286 (2006) 487.
[43] Z. Luo, H. Li, H. Shu, K. Wang, J. Xia, Y. Yan, Cryst. Growth Des. 8 (2008) 2275–2281.
[44] A. Cameirão, R. David, F. Espitalier, F. Gruy, J. Cryst. Growth 310 (2008) 4152–4162.